

Multi-Wavelength Studies of Spectacular Ram Pressure Stripping of a Galaxy: Discovery of an X-ray Absorption Feature

Liyi Gu^{1,2}, Masafumi Yagi³, Kazuhiro Nakazawa⁴, Michitoshi Yoshida⁵, Yutaka Fujita⁶, Takashi Hattori⁷, Takuya Akahori⁸, Kazuo Makishima^{1,4,9}

ABSTRACT

We report the detection of an X-ray absorption feature near the galaxy M86 in the Virgo cluster. The absorber has a column density of $2 - 3 \times 10^{20} \text{ cm}^{-2}$, and its position coincides with the peak of an intracluster H I cloud which was removed from the galaxy NGC 4388 presumably by ram pressure. These results indicate that the H I cloud is located in front of M86 along the line-of-sight, and suggest that the stripping was primarily created by an interaction between NGC 4388 and the hot plasmas of the Virgo cluster, not the M86 halo. By calculating an X-ray temperature map, we further detected an X-ray counterpart of the H I cloud up to $\approx 3'$ south of M86. It has a temperature of 0.89 keV and a mass of $\sim 4.5 \times 10^8 M_{\odot}$, exceeding the estimated H I gas mass. The high hot-to-cold gas ratio in the cloud indicates a significant evaporation of the H I gas, probably by thermal conduction from the hotter cluster plasma with a sub-Spitzer rate.

¹Research Center for the Early Universe, School of Science, University of Tokyo, 7-3-1, Hongo, Bunkyo-ku, Tokyo 113-0033, Japan; lygu@juno.phys.s.u-tokyo.ac.jp

²Department of Physics, Shanghai Jiao Tong University, 800 Dongchuan Road, Shanghai 200240, PRC

³Optical and Infrared Astronomy Division, National Astronomical Observatory of Japan, 2-21-1, Osawa, Mitaka, Tokyo, 181-8588, Japan

⁴Department of Physics, University of Tokyo, 7-3-1, Hongo, Bunkyo-ku, Tokyo 113-0033, Japan

⁵Hiroshima Astrophysical Science Center, Hiroshima University, 1-3-1, Kagamiyama, Higashi-Hiroshima, Hiroshima, 739-8526, Japan

⁶Department of Earth and Space Science, Graduate School of Science, Osaka University, 1-1 Machikaneyama-cho, Toyonaka, Osaka 560-0043, Japan

⁷Subaru Telescope, National Astronomical Observatory of Japan, 650 North A'Ohoku Place, Hilo, HI 96720, USA

⁸Sydney Institute for Astronomy, School of Physics, The University of Sydney, NSW 2006, Australia

⁹MAXI Team, Institute of Physical and Chemical Research, 2-1 Hirosawa, Wako, Saitama 351-0198, Japan

1. INTRODUCTION

Ram pressure stripping (RPS hereafter) by intracluster medium (ICM; namely, X-ray emitting hot plasma in clusters of galaxies) is one of the major mechanisms of gas removal from cluster member galaxies (e.g., Gunn & Gott 1972; Fujita & Nagashima 1999). The galactic materials, thus removed from the galaxies, form tail-like structures behind, which have been observed in, e.g., H I (e.g., Vollmer & Huchtmeier 2007), H α (e.g., Yoshida et al. 2012), and X-ray bands (e.g., Sun et al. 2010). Such a gas removal process may quench the star formation in galaxies, and expedite morphological transformation from spirals to S0s (e.g., Fujita & Nagashima 1999; Poggianti et al. 1999). This provides a plausible explanation to the observed environmental effects of cluster galaxies (e.g., Dressler 1980). However, details of the RPS process are not yet clear from observational viewpoints, leaving a significant uncertainties in the current theoretical modelings.

One of the best candidates for the observational RPS study is a nearby spiral galaxy NGC 4388 (N4388 hereafter). It is located at a projected distance of 1.3 degree away from the core of the Virgo cluster (M87), and its radial velocity of ≈ 2525 km s $^{-1}$ is about by 1500 km s $^{-1}$ higher than that of M87. Such a high velocity is thought to have enhanced the RPS in this object. In fact, as reported in, e.g., Kenney & Young (1989) and Cayatte et al. (1990), N4388 is one of the most H I-deficient spiral galaxies in the Virgo cluster. Recently, more intriguing RPS features have been unveiled: Yoshida et al. (2002) discovered in H α a plume of ionized gas extending 35 kpc to the northeast. Moreover, as shown in Oosterloo & van Gorkom (2005, hereafter OG05), the stripped plume has an H I counterpart with a larger extent of about 110 kpc ($\approx 24'$), containing a mass of about $3.4 \times 10^8 M_{\odot}$ in the atomic phase. Using an X-ray imaging analysis, Weżgowiec et al. (2011) found an X-ray counterpart associated with the H α and H I tails.

As suggested in, e.g., Vollmer & Huchtmeier (2003), the stripping may be due to an interaction with the ICM of the Virgo cluster at a projected distance of ~ 350 kpc from M87. In contrast, OG05 and Vollmer (2009) proposed an alternative view: N4388 is interacting, at a speed > 2800 km s $^{-1}$, with the hot gas halo of the M86 group which is assumed to be located outside the Virgo cluster. Since M86 has a projected distance of only ~ 10 kpc from the plume, they can actually be very close in three dimensions. Due to large systematic uncertainties on the line-of-sight distance of N4388 (e.g., 13.6 Mpc from Schoeniger & Sofue 1997; 19.2 Mpc from Willick et al. 1997; and 38.7 Mpc from Theureau et al. 2007), the origin of the stripping in N4388 remain unclear.

The cold H I plume, which has a column density sufficient to significantly absorb background X-ray photons, is found covering an X-ray bright, $\sim 15' \times 5'$ field in the central $20'$ region of the M86 group (OG05). This makes the X-ray absorption measurement a promising

way to constrain the line-of-sight geometry between N4388 and M86. For this purpose, we carried out a spatially resolved X-ray spectroscopic analysis on the M86-N4388 region. We assume a distance of 16.7 Mpc to the Virgo Cluster, so that $1'$ corresponds to about 4.86 kpc. For easy calculation, the same values are assumed also for N4388 and M86. Unless stated otherwise, the quoted errors are at the 90% confidence level.

2. OBSERVATION AND DATA REDUCTION

The M86 center and N4388 regions were observed with the European Photon Imaging Camera (EPIC) onboard *XMM-Newton*, on 2002 July 1 and 2011 June 17, respectively. The combined field of view covers the entire H I cloud reported in OG05. Basic reduction and calibration of the EPIC data were carried out with SAS v12.0.1. In the screening we set *FLAG*=0, and kept events with *PATTERNS* 0 – 12 and 0 – 4 for the MOS and pn cameras, respectively. By examining lightcurves extracted in 10.0 – 14.0 keV and 1.0 – 5.0 keV from source-free regions, we rejected time intervals affected by hard- and soft-band flares, respectively, in which the count rate exceeds a 2σ limit above the quiescent mean value (e.g., Katayama et al. 2004). The obtained clean MOS(pn) exposures are 65(39) ks and 26(10) ks for the M86 and N4388 pointings, respectively. Point sources detected by a SAS tool *edetect_chain* were discarded in the spectral analysis.

Background was estimated as a combination of three independent components, i.e., instrumental background, cosmic X-ray background (CXB), and the Galactic emission. Following Gu et al. (2012), we created the instrumental background spectra for all the EPIC data using a filter wheel closed dataset. The CXB and Galactic emission components were calculated by analyzing spectra extracted from a region near the CCD edge of the N4388 pointing, which is about $7' - 11'$ south of N4388 ($25' - 30'$ west of M87). Specifically, we first subtracted the instrumental background from the extracted spectra, and then fitted the resulting spectra with a model consisting of three components; an absorbed power law model (photon index $\Gamma = 1.4$) describing the CXB, an absorbed optically thin thermal model with a temperature fixed at 0.2 keV and abundance at $1.0 Z_{\odot}$ for the Galactic foreground, and another absorbed thermal model for the projected ICM. A same absorption column density (N_{H} hereafter) was applied to the three components. The best-fit temperature of the ICM component is 1.6 ± 0.1 keV, which is consistent with the previous measurements (e.g., Ehlert et al. 2013). These fits constrained the 2.0 – 10.0 keV CXB flux as 7.4×10^{-8} ergs $\text{cm}^{-2} \text{s}^{-1} \text{sr}^{-1}$, which agrees with other reportings (e.g., Bautz et al. 2009). Adopting the CXB brightness uncertainty of 6.2% for a 0.5 deg^2 region reported in Kushino et al. (2002), we include a CXB systematic error of 12% in subsequent analysis. It was combined

in quadrature with a statistical uncertainty, which was calculated by scanning over the parameter space with the XSPEC command *steppar*, to constitute the total measurement errors in the spectral fittings.

3. ANALYSIS AND RESULTS

3.1. Excess Neutral Absorption

In order to search the X-ray data for possible absorption features associated with the atomic gas cloud, we calculated a 2-D absorption map of the M86 central region based on a centroidal Voronoi tessellation (CVT hereafter; Cappellari & Copin 2003) binning method. The $20'.1 \times 20'.1$ region shown in Figure 1a was thus divided into 71 sub-regions, each having a minimal signal-to-noise ratio of 100, or a count of ≥ 10000 in $0.4 - 7.0$ keV. Then we extracted the MOS and pn spectra from individual CVT sub-regions and fit them simultaneously in $0.4 - 7.0$ keV with an absorbed APEC model for the hot gas component, plus an absorbed power-law with index of 1.6 for unresolved point sources (e.g., X-ray binaries; Irwin et al. 2003) belonging to the galaxies. The redshift was fixed to 0, while the absorption, temperature, and metal abundance were set free. Adopting the redshift of N4388 (i.e., 0.008) does not change the fitting results. The obtained absorption map is shown in Figure 1b. The associated errors are typically $0.8 \times 10^{20} \text{ cm}^{-2}$ for low absorption sub-regions, and $1.0 \times 10^{20} \text{ cm}^{-2}$ for the higher ones. We also attempted to apply the same spectroscopic method to the EPIC data within $6'$ from the center of N4388; however, given the current data quality, we were not able to identify significant absorption structure beyond errors. Other datasets in *Chandra* and *Suzaku* archives are not suited for this purpose.

As shown in Figure 1b, the absorption N_{H} are in most regions consistent within errors with the Galactic value (i.e., $2.84 \times 10^{20} \text{ cm}^{-2}$; Kalberla et al. 2005) throughout the field, but we found a possible excess region $\sim 3' - 7'$ southeast of the M86 center, as indicated by the red and purple circles. To verify this excess absorption structure (EAS hereafter), we investigated, in details, five representative regions on and surrounding the structure. The extracted pn spectra are shown in Figure 2a. One of them (gray) is inferred to have a slightly lower temperature, as suggested by its lower spectrum peak energy than in the others. The remaining four exhibit similar spectra in ≥ 0.8 keV, but two of them (red and purple) show lower fluxes at < 0.8 keV than the other two, suggesting different absorption N_{H} . To quantify these inferences, the extracted spectra were fit with the same absorbed APEC + power-law model as plotted in Figure 2b. The obtained confidence contours are plotted in Figure 2c and 2d, on the absorption versus temperature, and absorption versus power-law normalization planes, respectively. It shows that the absorption on the EAS (red and purple

circles; $\geq 5 \times 10^{20} \text{ cm}^{-2}$) is higher than those of the surrounding regions ($\sim 3 \times 10^{20} \text{ cm}^{-2}$) at the 90% confidence level, which cannot be ascribed to uncertainties in the gas temperature or point source measurements. As shown in Cortese et al. (2010), there is no significant Galactic dust cloud near the EAS region, indicating that the excess absorption cannot be created, either, by foreground absorption inhomogeneity.

To take into account the projected Virgo ICM component, we fit the spectra from the EAS by adding a second absorbed APEC model. According to previous measurement in Urban et al. (2011), the temperature of the Virgo component was fixed at 2.3 keV. The two-phase model gave a better fit ($\chi^2/\nu = 315/279$) than the single-phase one ($\chi^2/\nu = 345/280$) to the northeast part of the EAS (purple circle in Fig. 1). It yielded a temperature of 0.8 ± 0.1 keV for the M86 component, and a smaller overall absorbing N_{H} of $3.8 \pm 0.6 \times 10^{20} \text{ cm}^{-2}$ (Fig. 2c). According to the XSPEC tool `simftest`, the fitting improvement with the two-phase model is significant at $> 99\%$ confidence level. Although the two-phase model might partially explain the observed N_{H} in the purple region, the excess absorption remains essentially unchanged in the red one. To further explore the origin of the EAS in the red region, we allowed the absorptions of the two-phase components to vary freely. The best-fit N_{H} are $5.4 \pm 1.0 \times 10^{20} \text{ cm}^{-2}$ and $< 3.7 \times 10^{20} \text{ cm}^{-2}$ for the M86 and Virgo components, respectively. This implies that the measurement of the EAS is driven by the M86 emission. Such a two-phase model was also applied to the surrounding non-EAS regions (gray, black, and blue circles in Fig. 1), and the resulting N_{H} are consistent with, or smaller than, the single-phase ones.

Then we compared the detected EAS with the H I tail reported in OG05. As shown in Figure 1b, the southwest part of the EAS nicely coincides with the peak of the H I emission. The excess X-ray absorption N_{H} above the Galactic value, $2 - 3 \times 10^{20} \text{ cm}^{-2}$, is consistent with that estimated from the radio data ($\geq 1 \times 10^{20} \text{ cm}^{-2}$; OG05). Also, based on the two-phase results of the red and purple circles, the mass of the absorber is estimated to be $2 - 3 \times 10^8 M_{\odot}$, which agrees with the H I mass ($3.4 \times 10^8 M_{\odot}$). These indicate that the southwest EAS is probably induced by the H I tail. On the other hand, the northeast part of the EAS (purple circle), which exhibits an excess absorption of $\sim 1 \times 10^{20} \text{ cm}^{-2}$ (according to the two-phase fit), appears in a more complicated region. Besides the northeast tip of the H I tail, a plume of ionized gas, which has been found extending NEE towards another galaxy NGC 4438 (e.g., Kenney et al. 2008; Randall et al. 2008; Ehlert et al. 2013), also appears to overlap with this feature. Hence, the northeast part of the EAS might be caused by a superposition of different absorbers.

3.2. A Cool X-ray tail

To investigate thermal structure of the hot gas in the H I tail, we have also created a 0.5 – 2.0 keV surface brightness map and a temperature map, shown in Figure 3a and 3b, respectively, both covering the M86 center and N4388 regions. The maps were calculated by the same CVT binning and spectral fitting methods as described in §3.1. Figure 3a reveals an X-ray emission enhancement (marked with a green box), by a factor of ~ 3 higher than the surrounding, extending from N4388 up to $\approx 3'$ south of M86. It is associated apparently with the H I tail. As shown in Figure 3b, the enhancement, or a tail, has a lower temperature, $kT = 1.07 \pm 0.08$ keV, than the surrounding region (≈ 1.31 keV) at the 99% confidence level.

To remove the projection effects, we carried out a two-phase spectral fitting to the low-temperature region shown in Figure 3b. Since the projected emission is likely to be a blend of both Virgo and M86 components, the temperature of the second APEC component was set free. This model did not give a significant improvement to the fitting ($\chi^2/\nu = 220/200$ compared to the single-phase $\chi^2/\nu = 228/202$), and the parameters of the two APEC components cannot be well constrained. This may be caused by a relatively poor data quality. We thus fixed the temperature of one component to the averaged surrounding value of 1.31 keV; then, the other temperature was obtained as 0.89 ± 0.10 keV. The 1.31 keV component has a surface brightness of $\approx 3.0 \pm 0.7 \times 10^{-14}$ ergs cm $^{-2}$ s $^{-1}$ arcmin $^{-2}$ in 0.5 – 7.0 keV, consistent with the surrounding value. Hence, the 0.89 keV component is naturally considered as local emission possibly associated with the tail. Assuming a cylinder shape (45 kpc in length and 10 kpc in radius) of the extracted region shown in Figure 3b, the density of the 0.89 keV component was calculated to be $\approx 1.2 \pm 0.2 \times 10^{-3} \eta^{-0.5}$ cm $^{-3}$, where η is the volume filling factor, and its total mass in the extracted region is $\approx 4.5 \pm 0.8 \times 10^8 \eta^{0.5} M_{\odot}$. The temperature and density of the X-ray tail are consistent with those reported in Weżgowiec et al. (2011).

4. Summary and Discussion

Based on a 2-D spectral analysis using the *XMM-Newton* data, we detected a region with excess absorption ($\Delta N_{\text{H}} = 2 - 3 \times 10^{20}$ cm $^{-2}$) at a distance of $\sim 3' - 7'$ southeast of the M86 center. The southwest peak of the absorption structure apparently coincides with the peak of an H I gas tail which was probably removed from N4388 by ram pressure. Towards southwest of the H I peak, the excess X-ray absorption diminished, but we instead observed, along the H I tail, an excess X-ray surface brightness (by a factor of 3) and a temperature decrease (from ~ 1.3 keV to 0.9 keV), which reconfirm the findings of Weżgowiec et al. (2011). If this is attributed to emission from a hot plasma, we find a mass of $\sim 4.5 \times 10^8 M_{\odot}$.

The detection of the EAS allows us to constrain, more tightly than before, the stripping location of the long H I tail. Our results indicate that the EAS region of the H I tail is now in front of, or at similar distance to, the center of the M86 group. In contrast, the heliocentric recession velocity of the EAS ($\sim 2300 \text{ km s}^{-1}$; OG05) is much larger than that of M86 (-244 km s^{-1}). Thus it is natural to expect that these two objects are moving towards each other at $\geq 2500 \text{ km s}^{-1}$ along the line-of-sight. Furthermore, given an age of $\sim 200 \text{ Myr}$ (OG05), the EAS region of the tail should have been created at least 510 kpc in front of M86.

This further allows us to consider the origin of the RPS. Let us first examine a possible interaction between N4388 and the M86 group ICM, assuming that the M86 is much outside the Virgo ICM sphere. By extrapolating the radially-averaged emission measure profile shown in Figure 9 of Randall et al. (2008), the hot gas density of M86 at $r = 510 \text{ kpc}$ is $\approx 1 \times 10^{-5} \text{ cm}^{-3}$, and the ram pressure acted on N4388 is $\approx 1 \times 10^{-12} \text{ dyn cm}^{-2}$. Next we consider a N4388-Virgo interaction. By adopting the gas density profile reported in Figure 6 of Urban et al. (2011) and a predicted orbit of N4388 suggested in Vollmer (2009), the Virgo ICM near the stripping spot ($r = 420 \text{ kpc}$) has a density of $1.5 \times 10^{-4} \text{ cm}^{-3}$, and the ram pressure is $\approx 4 \times 10^{-12} \text{ dyn cm}^{-2}$. Although the radial velocity difference between M86 and N4388 is larger than the Virgo-N4388 one, the low ICM density of the M86 significantly reduces the estimated ram pressure in the former case. A third picture is that N4388 has been interacting with a combination of the M86 and the Virgo ICM, assuming that the M86 group is well in the Virgo cluster (Randall et al. 2008). Then the ram pressure is enhanced to $\approx 5 \times 10^{-12} \text{ dyn cm}^{-2}$, which is contributed mostly from the Virgo ICM. To create stripping, the ram pressure should exceed the gravitational restoring force in the galaxy which was estimated to be $\approx 2.5 \times 10^{-12} \text{ dyn cm}^{-2}$ in Veilleux et al. (1999). Hence, our current result suggests that the N4388-M86 interaction is insufficient for the RPS, and the H I tail was created mostly by colliding with the Virgo ICM.

Another interesting aspect is to understand phase changes of the materials removed from N4388. Given the associated hot plasma mass and H I mass of $\sim 4.5 \pm 0.8 \times 10^8 \eta^{0.5} M_{\odot}$ (§3.2) and $3.4 \times 10^8 M_{\odot}$ (OG05), respectively, the ionized-to-atomic gas mass ratio in the tail is therefore ~ 1 , which is an order of magnitude higher than the typical values within disk galaxies (e.g., Rasmussen et al. 2009; Bigiel & Blitz 2012). It implies that the 0.89 keV plasma is not the ISM that was already in N4388 before the stripping, but rather a remnant of the cold gas, which has been transferred into the hot phase by thermal conduction or mixing with the ambient ICM. Let us examine the efficiency of the conductive heating. We may assume a minimal width of 5 kpc of the H I tail (Fig. 1 of OG05) and a N_{H} of $2 \times 10^{20} \text{ cm}^{-2}$ (§3.1). Then, employing a Spitzer rate conductivity, the evaporation timescale can be calculated to be $\sim 70 \text{ Myr}$, which is a factor of 3 shorter than the age of the tail. Hence, the thermal conduction should have been suppressed to some extent. This

can naturally be explained by some magnetic interfaces between the cold and hot phases. A similar scenario was proposed to explain the multi-phase hot plasmas in the cluster cD galaxy (e.g., Makishima et al. 2001; Gu et al. 2012). When the conductive heat to a magnetic-field structure is substantially blocked, its H I content might be condensed into star-forming materials. We will report this phenomenon in a follow-up paper.

Acknowledgments

We thank Tom Oosterloo and Jacqueline van Gorkom for providing us the H I map.

REFERENCES

- Bautz, M. W., Miller, E. D., Sanders, J. S., et al. 2009, PASJ, 61, 1117
- Bigiel, F., & Blitz, L. 2012, ApJ, 756, 183
- Cappellari, M., & Copin, Y. 2003, MNRAS, 342, 345
- Cayatte, V., van Gorkom, J. H., Balkowski, C., & Kotanyi, C. 1990, AJ, 100, 604
- Ciardullo, R., Jacoby, G. H., & Tonry, J. L. 1993, ApJ, 419, 479
- Ciardullo, R., Feldmeier, J. J., Jacoby, G. H., et al. 2002, ApJ, 577, 31
- Cortese, L., Bendo, G. J., Isaak, K. G., Davies, J. I., & Kent, B. R. 2010, MNRAS, 403, L26
- Dressler, A. 1980, ApJ, 236, 351
- Ehlert, S., Werner, N., Simionescu, A., et al. 2013, MNRAS, 430, 2401
- Ekholm, T., Lanoix, P., Teerikorpi, P., Fouqué, P., & Paturel, G. 2000, A&A, 355, 835
- Fujita, Y., & Nagashima, M. 1999, ApJ, 516, 619
- Fujita, Y., Tawa, N., Hayashida, K., et al. 2008, PASJ, 60, 343
- Gu, L., Xu, H., Gu, J., et al. 2012, ApJ, 749, 186
- Gunn, J. E., & Gott, J. R., III 1972, ApJ, 176, 1
- Irwin, J. A., Athey, A. E., & Bregman, J. N. 2003, ApJ, 587, 356

- Jordán, A., Blakeslee, J. P., Côté, P., et al. 2007, *ApJS*, 169, 213
- Kalberla, P. M. W., Burton, W. B., Hartmann, D., et al. 2005, *A&A*, 440, 775
- Katayama, H., Takahashi, I., Ikebe, Y., Matsushita, K., & Freyberg, M. J. 2004, *A&A*, 414, 767
- Kenney, J. D. P., & Young, J. S. 1989, *ApJ*, 344, 171
- Kenney, J. D. P., Tal, T., Crowl, H. H., Feldmeier, J., & Jacoby, G. H. 2008, *ApJ*, 687, L69
- Kushino, A., Ishisaki, Y., Morita, U., et al. 2002, *PASJ*, 54, 327
- Makishima, K., Ezawa, H., Fukuzawa, Y., et al. 2001, *PASJ*, 53, 401
- Oosterloo, T., & van Gorkom, J. 2005, *A&A*, 437, L19
- Poggianti, B. M., Smail, I., Dressler, A., et al. 1999, *ApJ*, 518, 576
- Randall, S., Nulsen, P., Forman, W. R., et al. 2008, *ApJ*, 688, 208
- Rasmussen, J., Sommer-Larsen, J., Pedersen, K., et al. 2009, *ApJ*, 697, 79
- Schoeniger, F., & Sofue, Y. 1997, *A&A*, 323, 14
- Sun, M., Donahue, M., Roediger, E., et al. 2010, *ApJ*, 708, 946
- Theureau, G., Hanski, M. O., Coudreau, N., Hallet, N., & Martin, J.-M. 2007, *A&A*, 465, 71
- Urban, O., Werner, N., Simionescu, A., Allen, S. W., Böhringer, H. 2011, *MNRAS*, 414, 2101
- Veilleux, S., Bland-Hawthorn, J., Cecil, G., Tully, R. B., & Miller, S. T. 1999, *ApJ*, 520, 111
- Villegas, D., Jordán, A., Peng, E. W., et al. 2010, *ApJ*, 717, 603
- Vollmer, B., & Huchtmeier, W. 2003, *A&A*, 406, 427
- Vollmer, B., & Huchtmeier, W. 2007, *A&A*, 462, 93
- Vollmer, B. 2009, *A&A*, 502, 427
- Weżgowiec, M., Vollmer, B., Ehle, M., et al. 2011, *A&A*, 531, A44
- Willick, J. A., Courteau, S., Faber, S. M., et al. 1997, *ApJS*, 109, 333

Yoshida, M., Yagi, M., Okamura, S., et al. 2002, *ApJ*, 567, 118

Yoshida, M., Yagi, M., Komiyama, Y., et al. 2012, *ApJ*, 749, 43

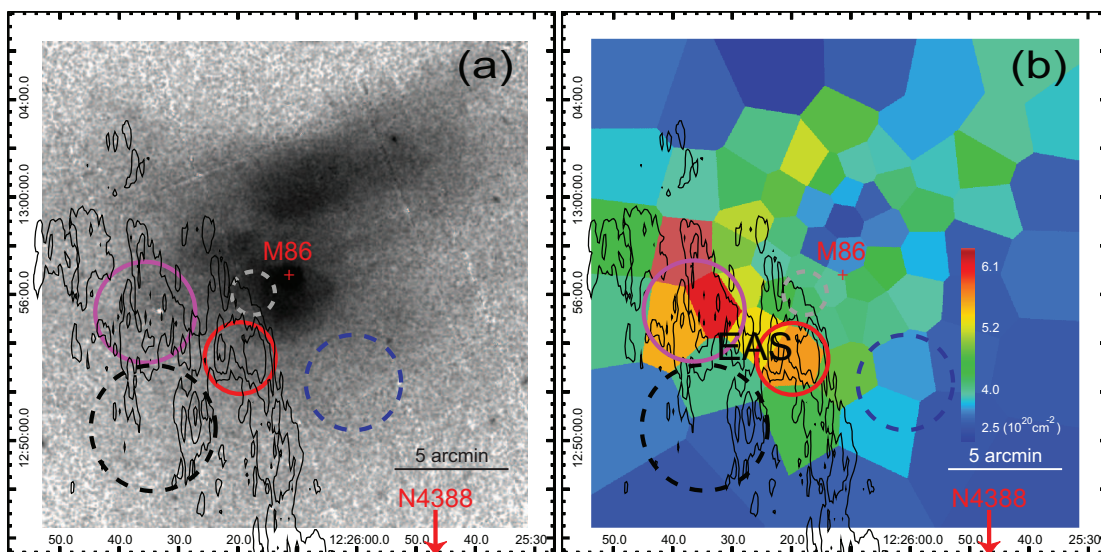


Fig. 1.— (a) A 0.5–2.0 keV exposure-corrected image of the M86 group. The H I brightness contours are overlaid in black, with contour levels of 1.0, 5.0, and 10.0 in units of 10^{19} cm^{-2} . The regions for detailed spectral analysis (§3.1) are shown with circles, where red and purple solid circles indicate southwest and northeast of the EAS, respectively, and gray, black, and blue dashed ones show the surrounding regions. (b) X-ray absorption map of the M86 central region. Errors are typically $0.8 \times 10^{20} \text{ cm}^{-2}$ for low absorption regions, and $1.0 \times 10^{20} \text{ cm}^{-2}$ for higher ones.

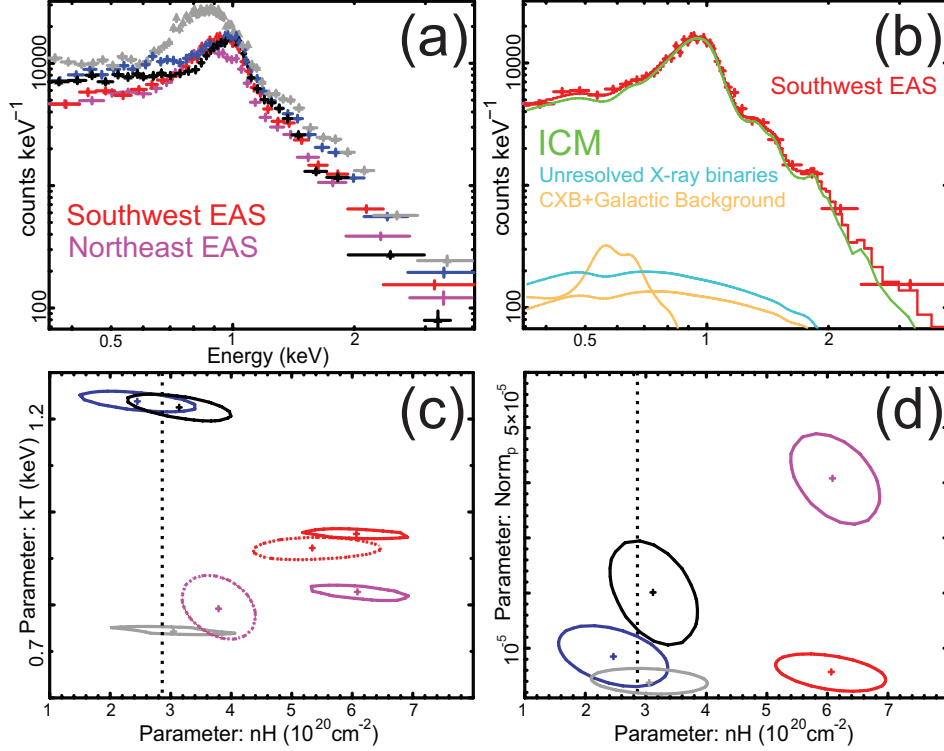


Fig. 2.— (a) EPIC-pn spectra of the five regions shown in Figure 1. The spectra are colored in the same way as the circles in Figure 1. (b) Best-fit single-phase models to the EPIC-pn spectrum of the southwest part of the EAS. The ICM, unresolved point source, and background components are shown in green, cyan, and orange, respectively. (c) Confidence contours between temperature and absorption at the 90% confidence level for the five regions. Solid and dotted contours indicate the results with single-phase and two-phase models. The temperatures of the cooler components are plotted in the two-phase cases. The Galactic H I column density is indicated by a dashed black line. (d) Confidence contours between the normalization of unresolved point source component and absorption obtained with the single-phase model at the 90% confidence level.

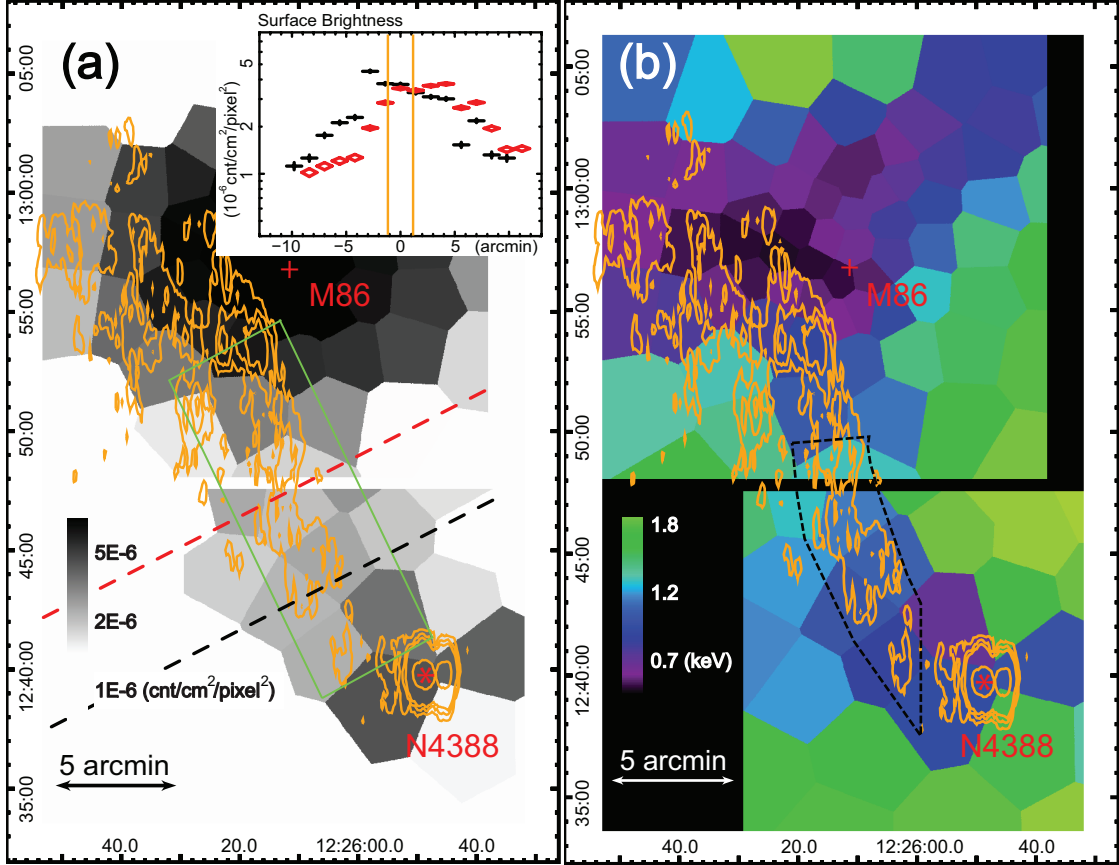


Fig. 3.— (a) A 0.5 – 1.0 keV exposure-corrected, background-subtracted surface brightness map of the M86-N4388 region. The H I brightness contours are overlaid in orange, and the centers of M86 and N4388 are shown with a red cross and a star, respectively. A green box indicate the region with enhanced X-ray brightness. Surface brightness profiles along the dashed red and black lines are shown in the insert, where the H I cloud is marked with vertical orange lines. 1×10^{-6} cnt cm $^{-2}$ pixel $^{-2}$ is about 2.7×10^{-14} ergs cm $^{-2}$ s $^{-1}$ arcmin $^{-2}$ in 0.5 – 7.0 keV. (b) A temperature map of the same region. The region used for detailed spectral analysis (§3.2) is marked with dashed black lines.